

RAPID PROTOTYPING FOR WIND TUNNEL TESTING AND INSTRUMENTATION

Richard Thomas
Whittle Laboratory
Cambridge University

Howard Hodson
Whittle Laboratory
Cambridge University

ABSTRACT

Recent developments in additive-based prototyping technologies now afford academic institutes and industry alike an accessible manufacturing process for the quick and cost-effective production of CAD geometries with sufficient surface tolerance and material strength as to be suitable for traditional wind tunnel testing. Furthermore, complex internal features such as pressure lines and cavities can be included in the CAD that, under more traditional manufacturing techniques, would prove challenging, if not impossible, to achieve. This paper assesses and compares the capabilities of available additive rapid prototyping technologies, including Fused Deposition Modelling, Stereolithography, Three-Dimensional Printing, Mask Projection and Jetted Photopolymer techniques. A common sample part has been produced using each of the above prototyping techniques from various manufacturers. The geometrical tolerance and surface quality of each part has been assessed, alongside the properties of a selection of materials available to each machine, and the suitability of each technique to the production of instrumented wind tunnel models is discussed. In addition, Direct Metal Laser Sintering has been used to produce blades with internal cooling systems and aerodynamic probes.

INTRODUCTION

Rapid Prototyping is fast becoming a cost-effective technique for the speedy manufacture of complex components. Intense competition between several leading companies has reduced the purchase and operational costs of smaller, office-based, rapid prototyping machines. Subsequently the affordability of rapid prototyping technologies is reaching a level where ordinary academic institutions can begin to consider the purchase of a RP machine for in-house manufacturing.

Several techniques are benchmarked in this study to determine the suitability of a variety of rapid prototyping technologies to wind tunnel testing and instrumentation. A common test part has been designed and manufactured on each of the machines, and subsequently assessed to determine its geometrical accuracy and model fidelity.

All of the tested rapid prototyping (RP) techniques reported in this paper build models using variations of a simple layer building principle. First, the model is discretized into many thin horizontal slices. Then, each slice is systematically created from either the solidification of a UV sensitive liquid resin or the bonding of an accurately deposited strand of solid plastic. By building each layer on top of the previous, the three-dimensional model is slowly realised slice-by-slice. The result approximates to the original CAD model with an accuracy that is determined by the machine's digital resolution and tolerances

RESULTS AND DISCUSSION

Rapid Prototyping Techniques

Fused Deposition Modelling

The technique of Fused Deposition Modelling builds each slice by first laying down an outline in very fine lengths of softened plastic and then cross-filling the internal volumes. Parts can be manufactured with a soluble support structure that leaves no surface artefacts, and internal pressure lines are faithfully reproduced. Drawbacks include model porosity, and a relatively large minimum layer thickness. Fusion of the layers during manufacture is not completely effective, resulting in a model with a porous skin. Dipping the model in a solution of methyl-ethyl-ketone (MEK) encourages further binding of each layer, however tests showed that this did not sufficiently seal the layers as leaks occurred between neighbouring pressure lines. A third test part, subjected to a recently developed vapour cloud dipping process, demonstrated much lower surface porosities. However, it remained non-airtight and as such, although FDM parts are certainly a candidate for wind tunnel testing, they are not suitable for the inclusion of internal pressure lines.

Three-Dimensional Printing

Three-dimensional printing (3DP) builds parts by laying down a layer of powder which is then selectively glued using an adhesive solution where a solid model is required. Parts produced in 3DP are produced quickly and cheaply, but have been found to be too fragile for practical use in wind tunnel testing. Impregnating the surface with a hardened resin increased the model strength, but the parts remained fragile. Although geometrical accuracy was impressive, the surface quality was inadequate, with edges appearing rounded.

Digital Light Processing

Mask projection, or Digital Light Processing (DLP), techniques digitally project each slice of the model as an image onto a UV sensitive resin using standard light projection technology. Test parts were solid, having crisp sharp edges and a good material density. However, peculiar distortions were noticeable in parts manufactured in the materials SI500 and NanoCure, especially near a material over-hang. Here it is assumed that a lack of curing of the material during manufacture has led to parts deforming under their own weight. A post-curing UV oven intended to stiffen the model by fully curing the material seems to be an inadequate solution as our test parts retain visible levels of distortion. On the more positive side, material density is high creating non-porous models suitable for internal instrumentation, and a slightly translucent material is available to aid the process of cross-drilling surface tappings.

Jetted Photopolymer

The Objet jetted-photopolymer (JP) technique builds models from a UV sensitive resin, printing and curing the material directly in a similar manner to ordinary inkjet printing. The JP technique produced parts with sufficient geometrical accuracy and surface finish to qualify models for wind tunnel testing. Internal pressure lines are also faithfully reproduced, and the availability of a translucent material aids in cross-drilling these lines. However, the block-like support structure implemented by the Objet system can lead to one considerable problem; the removal of the support structure from internal pressure lines. This task can be impossible for particularly long and non-linear channel designs as attempts to remove the support material can result in the it becoming compacted within the channel and ultimately solidifying into a blockage.

Traditional Stereolithography

The word Stereolithography was originally coined to describe the traditional rapid prototyping process of curing a vat of UV sensitive resin with a precisely directed laser beam. This traditional technique appears to remain the current market leader in terms of model fidelity and material strength. Internal pressure lines can be accurately created, so long as any remaining liquid resin is ejected from the lines before it cures. Machines such as the Viper have a reported achievable layer thickness down to as low as 2.5 microns. Drawbacks include the need to remove surface artefacts from support structures, and the purchase and running costs of the machines.

Laser Sintering

Alternatives, including Selective Laser Sintering and Direct Metal Laser Sintering, also promise high surface finishes and geometrical accuracies. A simple five-hole probe model has been manufactured using DMLS demonstrating that an intricate pressure measurement device can be manufactured by RP techniques that require little to no surface finishing. An assessment of this rapid prototyped five-hole probe will be discussed later in this paper.

Test Part Assessment

For each of the rapid prototyping techniques listed above, excluding Laser Sintering, we produced a common test part, as shown in Figure 1. The part consists of many features, each designed to assess different aspects of a machine performance. The part consists of elongated overhangs, slanted surfaces, both shallow and steep, flats, small features (five hole probe inset) and internal channels. Each test part was assessed for its model fidelity, surface flatness, surface finish, small-feature accuracy and general geometrical tolerance. A geometrical error quotient, calculated from the RMS of several dimensional differences with respect to the model, was calculated to represent the accuracy of the model.

Furthermore, to understand the porosity of the materials and hence determine their suitability for internal instrumentation, each part was subjected to a porosity test. In this test one of the internal channels representing an instrumentation line is pressurized and the model submerged in water. Materials with a porous nature are revealed by the emergence of bubbles from the model skin and more noticeably the neighbouring channels.

Discussion of Rapid Prototyping Techniques

The RP technique of FDM produced two surprisingly impressive test parts (Figures 2 and 3). The test part from the relatively inexpensive Dimension SST showed the lowest geometrical error quotient, but with large layer thickness resulted in a model with a poor surface finish and insufficient small-feature accuracy. The more moderately priced Stratasys FDM 360, having a finer layer thickness capability, created a better surface finish

than the cheaper Dimension, but had a poor geometrical error quotient. This is believed to be due to a recently developed vapour-dipping process designed to seal the 'skin' of the part to achieve a watertight model. The dipping process partly dissolves the surface material to increase bonding between the layers, however geometrical defects begin to show, particularly at corners and in small feature areas. Furthermore, the dipping process was found to be ineffective in the internal channels of the model, as both FDM parts failed the porosity test. Figure 4 shows the emergence of air from neighbouring internal channels, demonstrating an internal leak.

The least expensive of the RP techniques studied here is the 3DP technology. Although producing a part with an impressively low geometrical error quotient of just 0.101 mm, the test part proved to be very fragile with a crumbly surface texture. The part is shown in Figure 5. The fragility of 3DP parts is a consequence of the powder binding technique, and subsequent strengthening processes are available to increase the versatility of produced parts, however these remain to be no more than a simple surface treatment. Given the part sits suspended during manufacture in a vat of its own powder material, surface fidelity is very good, and the larger few of the internal instrumentation channels were successfully created, but the material is most certainly porous.

Mask Projection (DLP) techniques from EnvisionTec produced two promising test parts, one in SI-300 and one in NanoCure (Figures 6 and 7). The NanoCure part proved the better of the two materials, demonstrating excellent model accuracy, with a geometrical error quotient of 0.109 mm, and managing to create both the tiny 0.762 mm surface hole and the attached five hole probe feature in its entirety (although with insufficient resolution to render it useable), as shown by the zoomed view of the tip in Figure 8. Both materials are watertight, and passed the porosity tests. Unfortunately, noticeable deviations in surfaces were apparent throughout both test parts. Of the many planar surfaces, many demonstrated bends, warps and deviations from flat, and indeed the stem of the attached five-hole probe was bent by a few degrees from base to tip (Figure 8).

The popular technique of Jetted Photopolymer, similar to inkjet printing technology, is available on the Eden 250 from Objet, a rapidly growing business aimed at the office-friendly rapid prototyping market. Their technology, although slower than most other processes, produces very accurate reliable parts with resolutions rivalled by only the more expensive industrial machines. Two test parts, produced in VeroWhite and FullCure720 (see Figures 9 and 10), a transparent material, performed well throughout all the tests, demonstrating excellent surface finish qualities, model fidelity and reasonable geometry error quotients. The transparency of the FullCure 720 material lends itself perfectly to the manufacture of internal instrumented wind tunnel models. The support structure is a gel-like block of scaffolding that entirely envelopes the model during production, and as such leaves no surface marks once carefully removed using pressurised water. The support structure does however need to be removed from internal channels, which presents a difficult, but not insurmountable, challenge.

Conclusions of Rapid Prototyping Techniques

FDM parts appear suitable for aerodynamic model making, but unsuitable for internal instrumentation channels. Dimension SST machine inexpensive, but requires plenty of surface finishing to achieve a smooth part. Stratasys FDM 360 more expensive, producing a finer quality part, but remains porous and unsuitable for internal instrumentation work. However, advantages include the availability of a soluble support material that leaves no surface marks or aberrations. This is clearly an advantage over other techniques such as DLP and JP.

3DP techniques produce weak parts unsuitable for wind tunnel testing or internal instrumentation. Although inexpensive, and having the capability of producing coloured models on the ZCorporation ZPrinter 450, material strength is low and consequently produced parts are most suited to more aesthetic applications.

The Mask Projection (DLP) technique of EnvisionTec proved to be a very promising technique, offering good surface finish, excellent small feature accuracy and a good solid material suitable for internal instrumentation work. However, an inability to produce planar surfaces reliably leaves one questioning the ability of the machine to accurately produce, for example, a critical aerodynamic surface.

The established JP technique, as adopted by Objet for their range of office-friendly Eden machines, has proven in these assessments to be a reliable technique, capable of meeting most of the requirements of wind tunnel part manufacture. Transparent watertight models can be accurately manufactured at high resolutions, with good surface finishes, suitable for internal instrumentation. A downside to the Objet Eden machines is the laborious removal of support material, which can take up to a few hours on more complex models.

Table 1 summarises some common properties of each machine and the test part properties.

Rapid Prototyping a Five-Hole Probe

In this section, the calibration of a 5-hole probe manufactured using the EOSINT Direct Metal Laser Sintering (DMLS) process is described. The machine places a 20 micron thick layer of metal powder evenly over the build area. A 250W CO₂ laser melts together the individual layers. Successive layers are created and this process is repeated until the part is completed. The quoted repeatable accuracy is +/-50 microns. The material used for the manufacture of the probe was a chromium steel. It was stated by the manufacturers that a

probe manufactured from this material would not be porous, whereas the alternative material (nickel-bronze) would be. The probe was built with its axis vertical.

Dominy and Hodson [2] reported the effects of changes in Reynolds number upon the calibrations of four different types of 5-hole cone probes. Three different cone angles (45° , 60° and 90°) and two hole geometries were investigated. The probes were calibrated at the exit from a transonic nozzle over a range of Reynolds numbers ($7 \times 10^3 < Re_d < 80 \times 10^3$) with additional information being obtained from calibrations obtained using a low speed open jet.

Two separate Reynolds number effects were identified by Dominy and Hodson [2]. The first was associated with separation of the flow from the probe body when the probe is at incidence. The effect upon the accuracy of the yaw measurement was limited to Reynolds numbers below 15×10^3 for a 90° cone probe. The hole geometry has little effect on these limits but it does influence the magnitude of the Reynolds number sensitivity. Designs where the yaw and pitch pressure holes were not perpendicular to the conical surface (so-called "forward facing" designs) were more sensitive to changes in Reynolds number. The second effect was most significant when the probe was nulled and extends to higher Reynolds numbers than does the effect of the leading edge separation. The dependence of the dynamic pressure coefficient upon Reynolds number under these conditions is such that the authors recommended that probes with forward facing pressure holes should not be employed in turbomachinery research. Dominy and Hodson also found that the probes with pressure holes drilled perpendicular to the conical surface shows that the probe with the largest cone angle (90°) was least sensitive to changes in Reynolds number.

Given the above findings, a 90° conical probe with the pressure holes perpendicular to the conical surface was designed. The probe design is shown in Figure 11(c), (d) and (e). This has a diameter at the measuring end of 2.0 mm and each pressure tapping is 0.3 mm in diameter. These dimensions are the same as those most often used at the Whittle Laboratory. The diameter of the probe is slowly doubled to 4.0 mm to enable 1.0 mm outside diameter stainless steel tubing to be soldered into the rear of the probe in order to provide the pressure connections to the instrumentation using plastic tubing. With a voxel size of 20 microns and a hole diameter of 0.3 mm, this geometry provided a challenge for the DMLS process.

In practice, the calibrations of two versions of the same probe were obtained. The first (see Figure 11(a)) was as supplied by the manufacturer but with the chamfer on the central hole improved by machining. The coarseness of the surface is a product of the manufacturing technique. The second (see Figure 11(b)) was produced by using a diamond grinding wheel to produce a smooth conical surface.

Five-Hole Probe Calibration Facility

The calibration was carried out using the Transonic Cascade Test Facility [1] of the Whittle Laboratory. This is a closed circuit, variable density ($0.04 < \rho < 3.5 \text{ kg/m}^3$) wind tunnel in which the Mach number and Reynolds number can be varied independently while the temperature is maintained at approximately ambient conditions.

For the purposes of the present investigation, the working section was fitted with half-open rectangular nozzle (Figure 12). The upper and lower walls are porous, which enables operation at supersonic conditions. Single-piece sidewalls extend beyond the exit of the upper and lower walls in order to permit the calibration of stem-mounted probes at up to 40 degrees of pitch. The height of the nozzle is 83 mm and the width is 101.6 mm. The geometry of the calibration nozzle is identical to that used by Dominy and Hodson [2].

The extended sidewalls are instrumented with static pressure tappings. The pressure tappings, spaced at a pitch of 6.35 mm, were fitted to both sidewalls along the centre-height of the tunnel (Figure 12, Figure 13). The probe under investigation was placed with its tip in the centre of the nozzle at the same axial location as the plane defined by the exit of the upper and lower walls. This location is the same axial location as that of the reference static pressure tapping. The pressures at this location, and several others in the vicinity of this reference tapping were measured during the experiment. There was very little variation along the axis of the tunnel in the vicinity of the probe. The stagnation pressure was measured in the upstream plenum. A T-type thermocouple was placed in the upstream plenum chamber for the determination of the inlet stagnation temperature. A 16-channel 15 psi common-differential Scanivalve DSA-3017 was used to measure the pressures. The reference-pressure for this unit was provided using the transducer in a 2 bar absolute Druck DPI-520 calibration unit.

The facility includes a computer controlled traversing and data acquisition system. Definitions of the pressure tappings of the probe and the yaw angle are given in Figure 14. Owing to the construction of the yaw and pitch mechanisms, the yaw angle is measured in the pitched plane (see Figure 14).

The Mach number is measured at each orientation of the probe. It is based upon the inlet stagnation pressure P_t and the reference wall-static pressure P_s measured at the same axial location as the side-tappings of the probe. The Mach number for all of the tests reported here was 0.9. This value was chosen because as sonic conditions are approached, small defects in the behaviour of a probe become exaggerated. The Reynolds number is based on the nominal probe size of 2.0 mm. The viscosity is determined using Sutherland's formulation and

the static temperature derived from the inlet stagnation temperature and the Mach number. The density is determined using the same basic measurements. All properties are assumed to be those for dry air. The Reynolds number was varied in the range from 4,000 to 35,000.

The calibration coefficients examined in this paper are defined as follows.

$$\begin{aligned} \text{Yaw coefficient (+ve for +ve angle)} & C_{yaw} = \frac{(P_2 - P_3)}{(P_1 - P_{ave})} \\ \text{Pitch coefficient (+ve for +ve angle)} & C_{pit} = \frac{(P_4 - P_5)}{(P_1 - P_{ave})} \\ \text{Total pressure coefficient} & C_t = \frac{(P_t - P_1)}{(P_1 - P_{ave})} \\ \text{Dynamic pressure coefficient} & C_d = \frac{(P_t - P_s)}{(P_1 - P_{ave})} \end{aligned}$$

where the psuedo-dynamic pressure is given by,

$$(P_1 - P_{ave}) = \frac{(P_1 - P_2) + (P_1 - P_3) + (P_1 - P_4) + (P_1 - P_5)}{4}$$

Five-Hole Probe Results and Discussion

Figure 15 and Figure 16 present the total pressure coefficients as a function of pitch angle for a range of yaw angles for the as-supplied and ground probe respectively. The response of the probes to yaw angle is almost symmetrical so only one half of the range of yaw angles that was tested is shown. The most significant result shown in Figure 15 and Figure 16 is that close to zero pitch and yaw, the stagnation pressure in the centre hole does not reach the true stagnation pressure. An examination of the probe revealed that this was due to porosity in the walls of the probe, which separate the internal pressure channels. As a consequence of this leakage, stagnation conditions are not achieved inside the central hole.

At high yaw and pitch angles, Figure 15 and Figure 16 show that the stagnation pressure coefficient of both probes increases, with the ground probe exhibiting a larger variation at high yaw and pitch angles. However, the ground probe has less sensitivity at smaller angles. It is also apparent that the highest total pressures measured by the ground probe occurred at a small negative angle of pitch. This is because, owing to the rough finish of the probe, it was not possible to locate the probe in the chuck of the grinder with sufficient accuracy to ensure that the axis of the cone was concentric with the axis of the probe.

Figure 17 and Figure 18 present the pitch coefficients as a function of pitch angle for a range of yaw angles for the as-supplied and ground probes respectively. The almost linear response to pitch angle is typical of a 90° conical probe. The pitch coefficient is almost independent of yaw. The reason why the ground probe shows a greater sensitivity to yaw angle is again due to the off-axis grinding.

The sensitivity of both probes to Reynolds number was almost identical. Figure 17 and Figure 18 present the total pressure and pitch coefficients as a function of pitch angle, at zero yaw angle, for a range of Reynolds numbers for the ground probe. There is little sensitivity of the pitch coefficients to the Reynolds number. This is in agreement with the findings of Dominy and Hodson for this design of probe. The total pressure coefficient exhibits what, at first sight, might be considered to be a strange phenomenon. Close to zero pitch, the coefficient increases as the Reynolds number decreases. This suggests that the leakage flow rate decreases with increasing Reynolds number. The reason for this is not know but it may indicate that the leakage flow is transitional.

The above discussion of Figure 15 to Figure 19 has shown that the two probes behave in a similar manner. Given the texture of the as-manufactured probe, the differences between them are sufficiently small that it is probably not necessary to grind the probe tip. Given the difficulty of doing this with sufficient accuracy, this is useful. Clearly, a non-porous product is required and it is possible that this can be achieved. In this case, the DMLS probe would represent a significant advance in pneumatic probe manufacturing.

REFERENCES

- [1] Gostelow, J.P. and Watson, P.J., "A closed circuit variable density air supply for turbomachinery research," ASME paper 76-GT-62, 1976.
- [2] Dominy, RG, and Hodson, HP, 1993, "An Investigation of Factors Influencing the Calibration of 5-hole Cone and Pyramid Probes", ASME Jnl of Turbomachinery, Vol 115, July , pp 513-519

FIGURES

	Objet Eden 250	Viper	Z Corporation Z Printer 310 Plus	3D Dimension SST 1200	EnvisionTec PerFactory	Stratasys FDM 360
Cost	£43k	£140k	£16k	£22.5k	£43k	£ 47k
Build Size (x,y,z) (mm)	260 x 260 x 200	250 x 250 x 250	203 x 254 x 203	254 x 254 x 305	230 x 172 x 230	355 x 254 x 254
Resolution (x,y,z)	42 x 84 x 16 µm	2.5 µm	300 x 450 dpi. Layer thickness down to 89 µm	Analogue X and Y. Layer thickness 254 µm	SXGA (1280 x 1024 pixels). Layer thickness better than 50 µm	Analogue X and Y. Layer thickness 127 µm
Material	Acrylic based translucent photopolymer	UV sensitive resin	A starch and cellulose- powder-based material, bonded with adhesive	ABS plastic	Liquid epoxy photopolymer methacrylate	ABD-M30
Support Structure	Gel-like support material. Leaves no surface artefacts	Same material. Leaves surface artefacts	No support material required.	Dissolvable support material. Leaves no surface artefacts	Same material. Leaves surface artefacts	Dissolvable support material. Leaves no surface artefacts
Surface Quality	Smooth flat surfaces with minimal stair-stepping	Smooth flat surfaces with minimal stair- stepping	Rough powdery surface finish	Rough hatched surface finish, very porous skin with ribbed sides	Smooth surface finish, with sharp edges	Hatched surface finish, porous skin with ribbed sides
Finishing	Surfaces require laborious hand finishing to remove support residue	Support structure removal and artefact cleanup	Finished parts from machine	Quick removal of soluble support structure	Support structure removal and artefact cleanup	Quick removal of soluble support structure
Pressure Lines	0.6 mm holes possible, although support material difficult to remove	1 mm holes possible. Occasional blockage due to curing of liquid	Material is porous, pressure lines not reliable	Model skin typically porous, pressure lines not reliable	0.3 mm holes possible with no support structure problems	Model skin typically porous, pressure lines not reliable
Material Properties	Strong but quickly becomes brittle under UV exposure	Strong – can be used for rotor blades	Weak – easily damages due to crumbly texture	Strong – near ABS plastic qualities. Layering introduces weaknesses	Strong – near ABS plastic qualities	Strong – ABS plastic qualities. Layering introduces weaknesses
Test Part Build Time	6 hours	14 hours	< 3 hours	5.3 hours	7 hours	15.1 hours

Table 1. Summary of various properties of each of the six rapid prototyping machines assessed

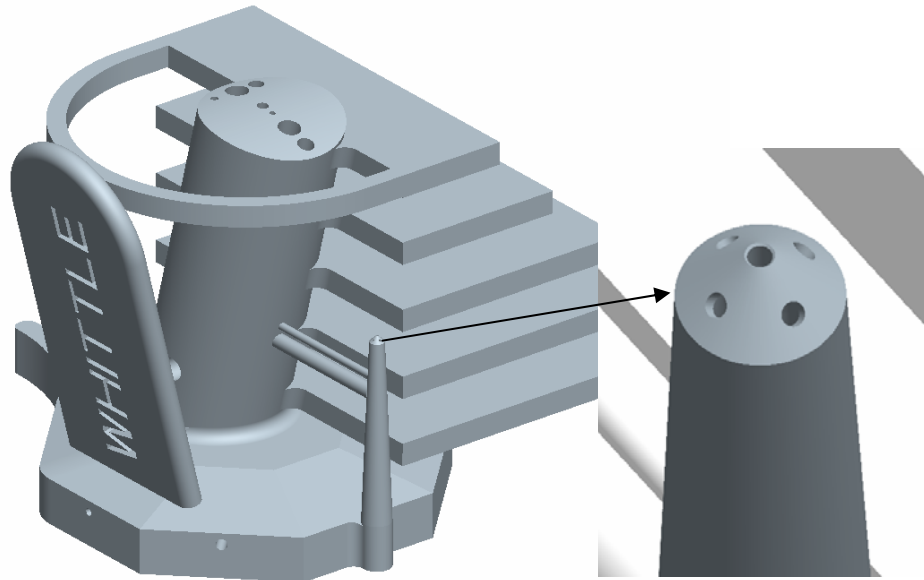


Figure 1. CAD Rendering of the Test Model



Figure 2. Dimension SST test part.

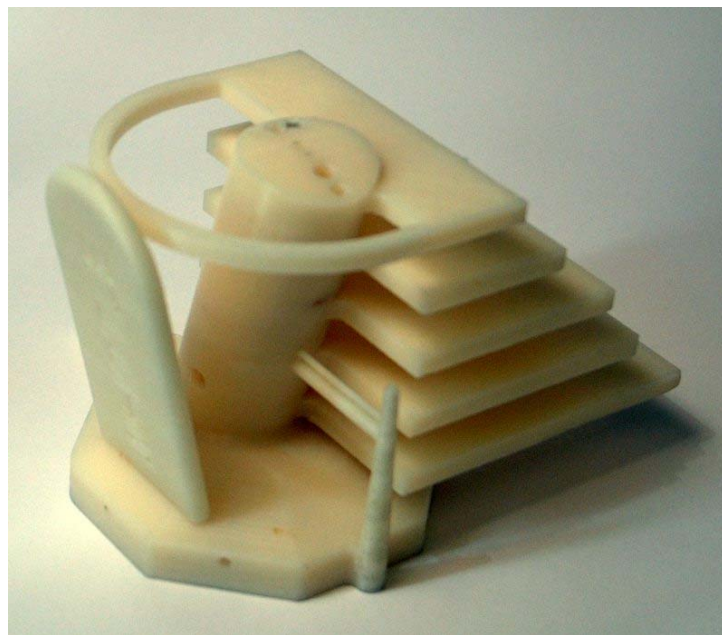


Figure 3. Stratasys FDM 360 test part.



Figure 4. The Stratasys FDM 360 part porosity test – notice the leakage of air from the three neighbouring internal channels demonstrating contamination between instrumentation lines.

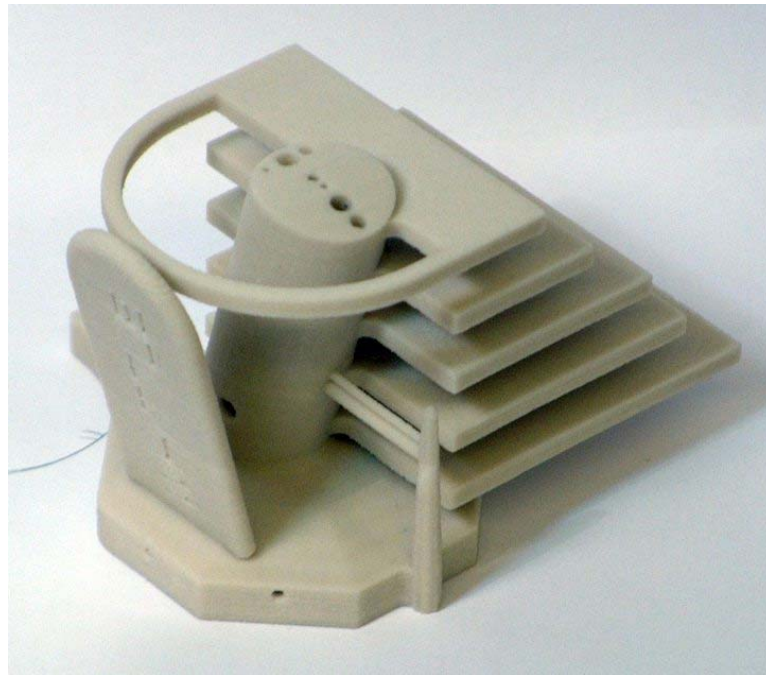


Figure 5. Dimension SST 3DP test part.



Figure 6. EnvisionTec SI-300 test part.

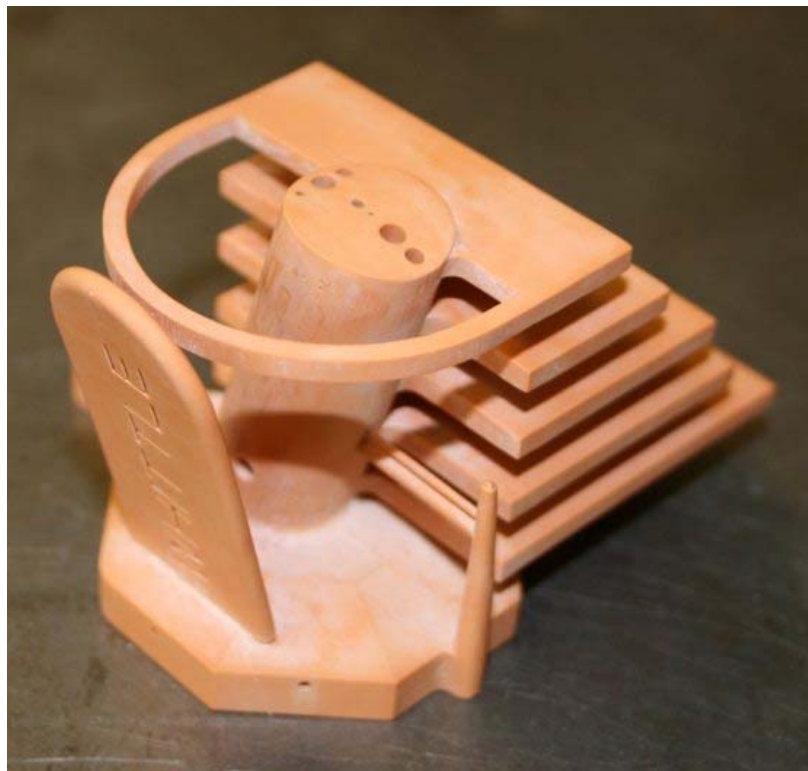


Figure 7. EnvisionTec NanoCure test part.

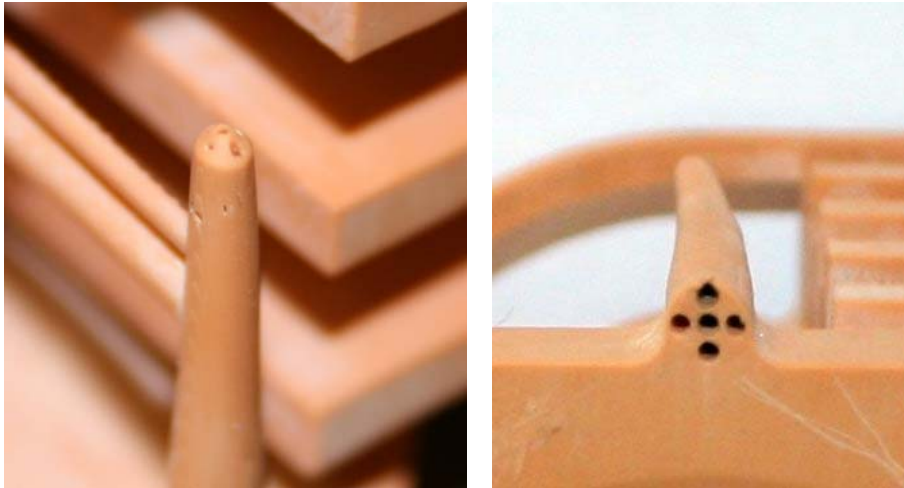


Figure 8. Detail view of the tip of the five hole probe feature on the EnvisionTec NanoCure test part, and along its length highlighting the distorted stem.

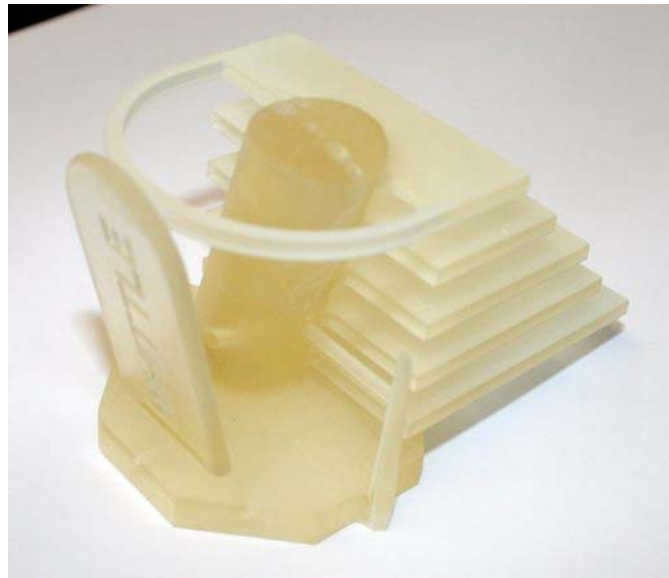


Figure 9. Objet FullCure 720 test part.

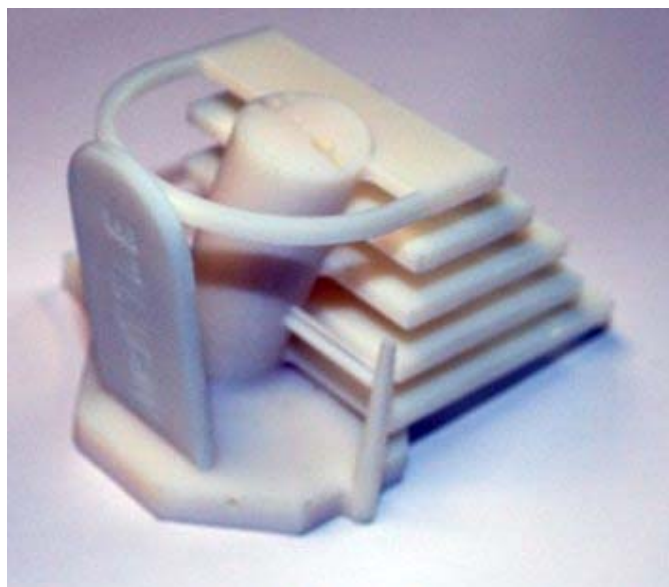


Figure 10. Objet VeroWhite test part.

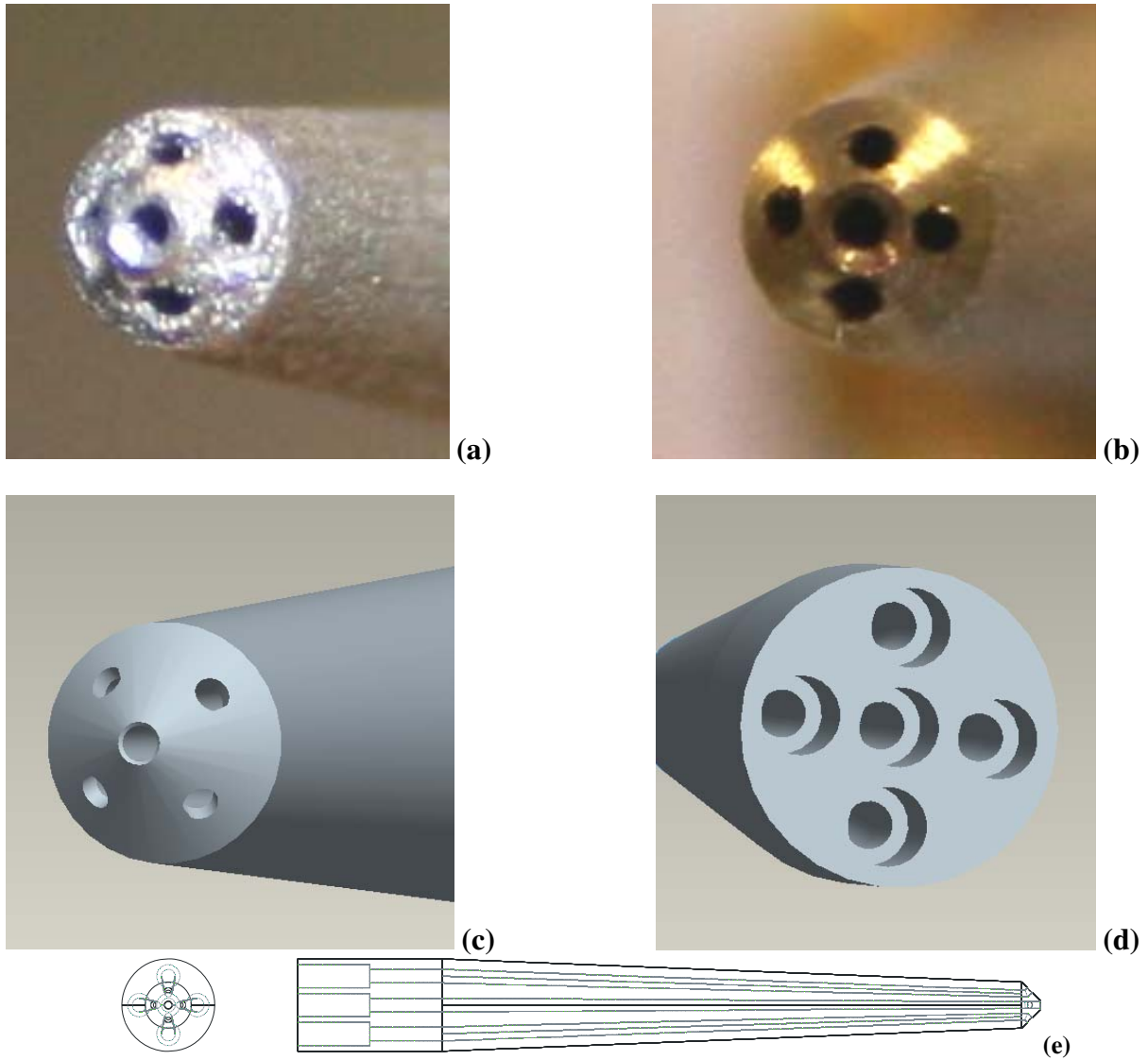


Figure 11. The probe geometry and the probe before and after grinding of the tip (a) Probe tip as manufactured (b) Probe tip after grinding of the conical surface (c) Probe tip as designed (d) Counterbores to accept stainless steel tubing for pressure connections (e) Drawing of probe.

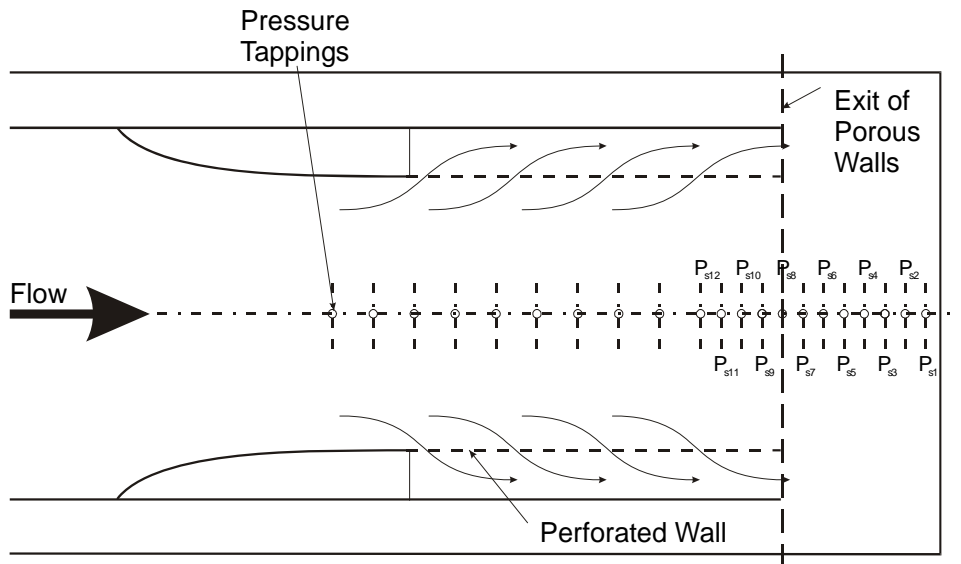


Figure 12. The calibration nozzle

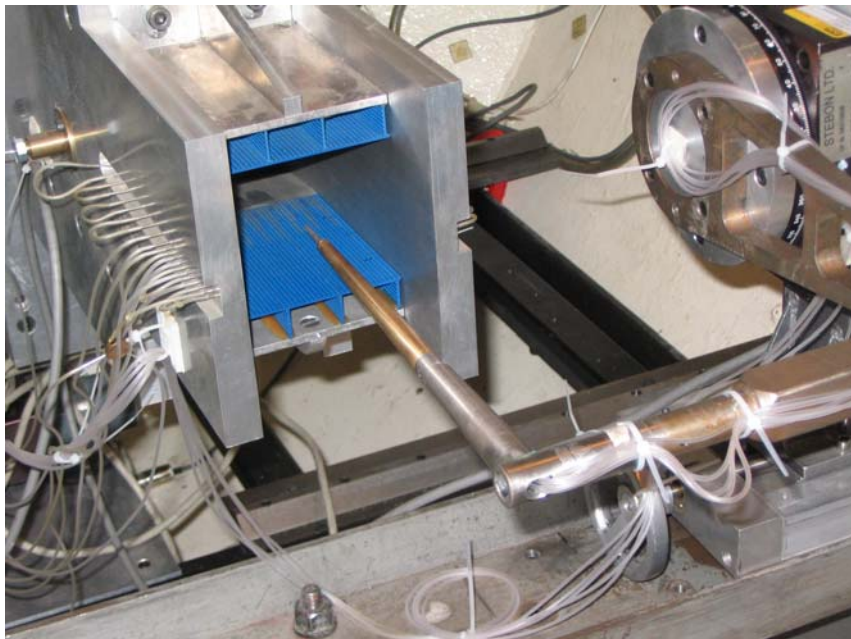


Figure 13. Probe in null position, traverse mechanism and calibration nozzle

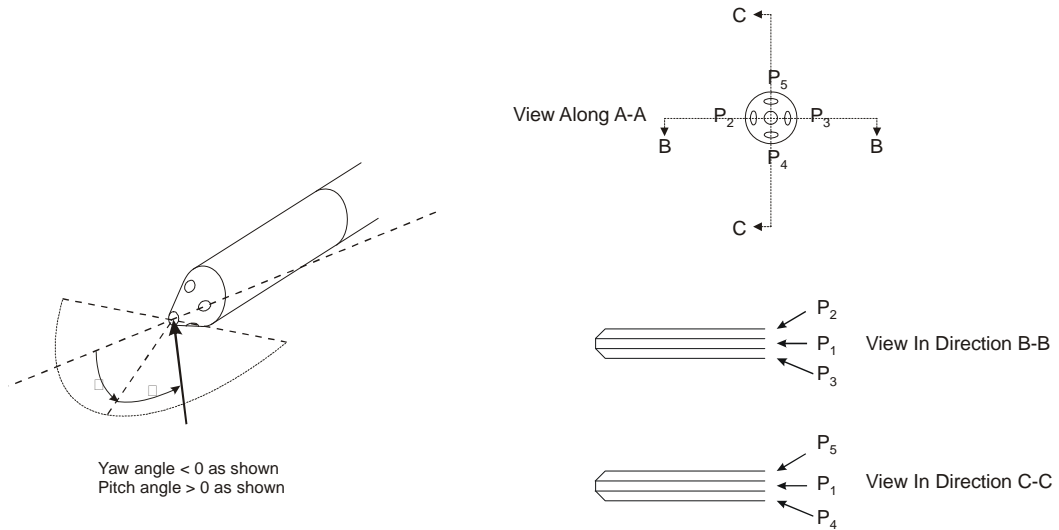


Figure 14. Definition of probe pressure tapings and angles

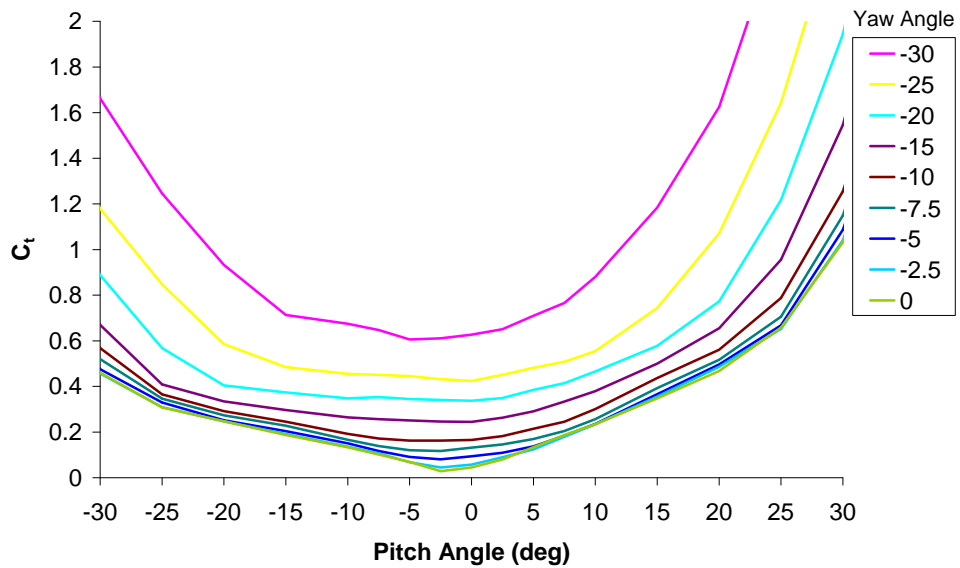


Figure 15. Total pressure coefficient for probe as supplied. Mach 0.9, Re=35,000, yaw angles = +/- 35°.

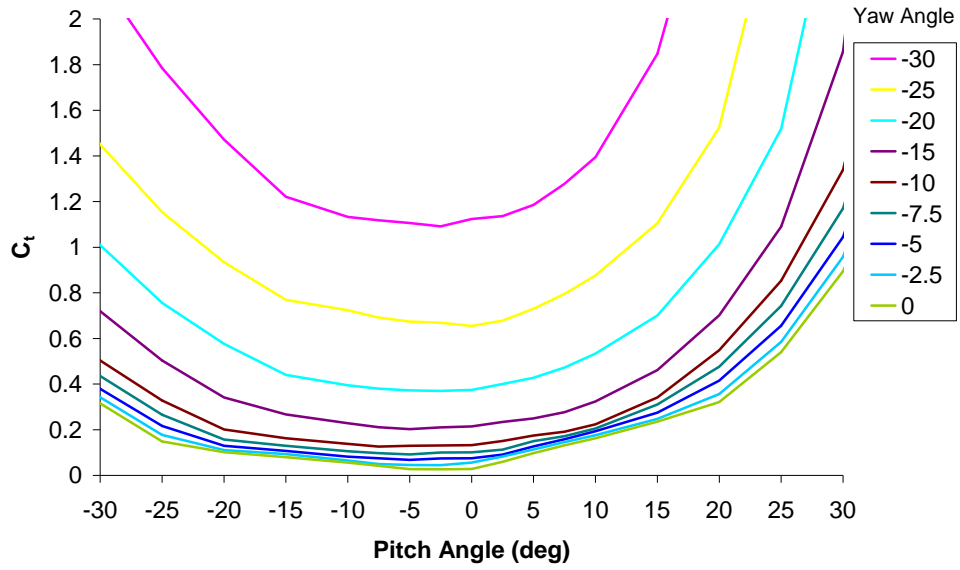


Figure 16. Total pressure coefficient for ground probe. Mach 0.9, $Re=35,000$, yaw angles = +/- 35°.

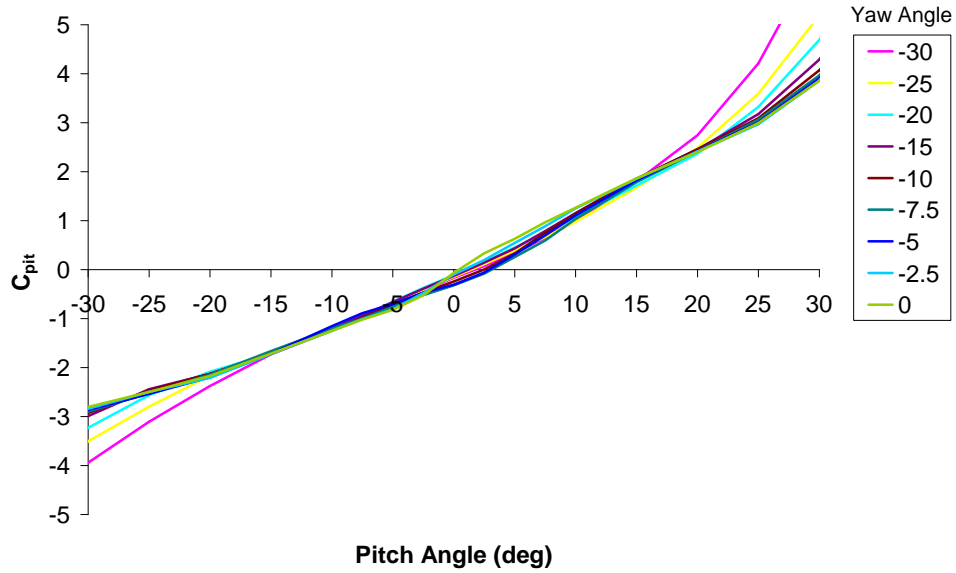


Figure 17. Pitch angle coefficient for probe as supplied. Mach 0.9, $Re=35,000$, yaw angles = +/- 35°.

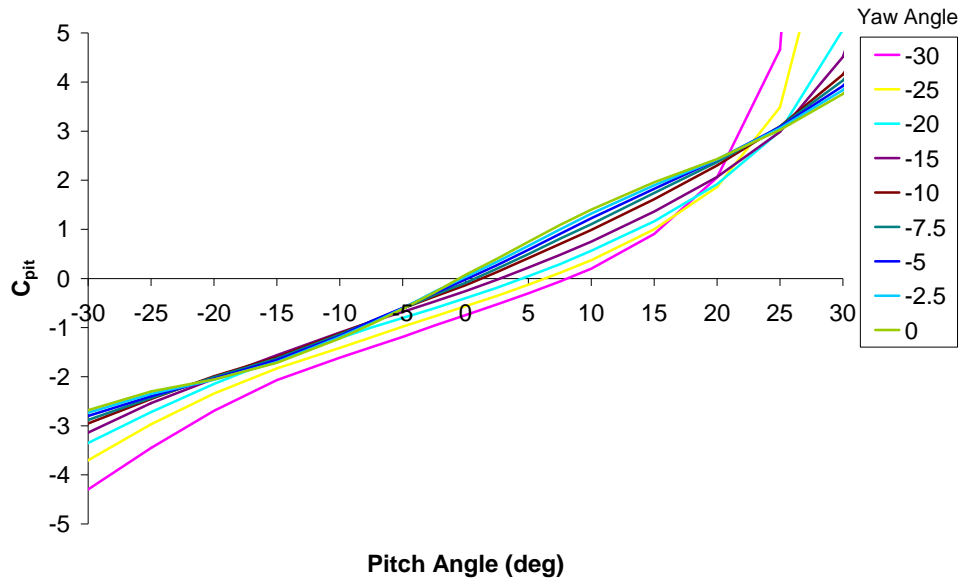


Figure 18. Pitch angle coefficient for ground probe. Mach 0.9, $Re=35,000$, yaw angles = +/- 35°.

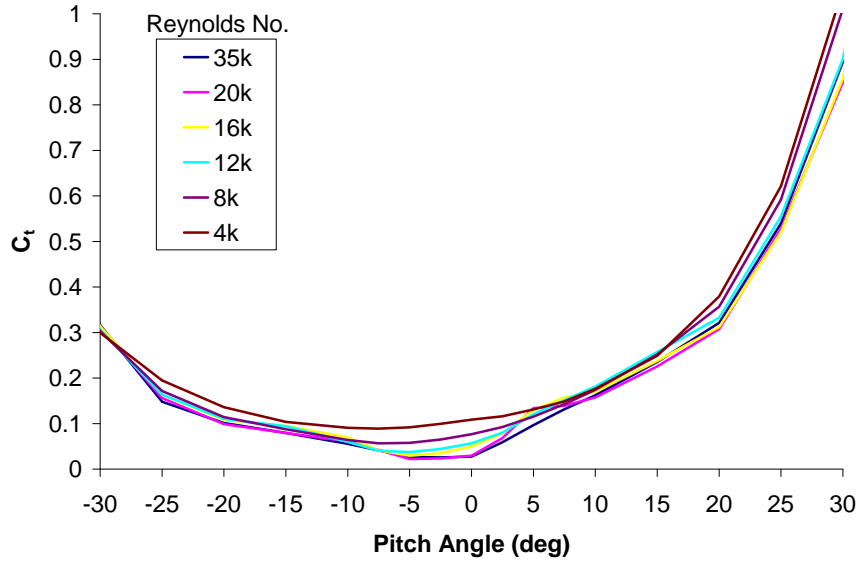


Figure 19. Total pressure coefficient for ground probe. Mach 0.9, $Re=4,000$ to 35,000, zero yaw.

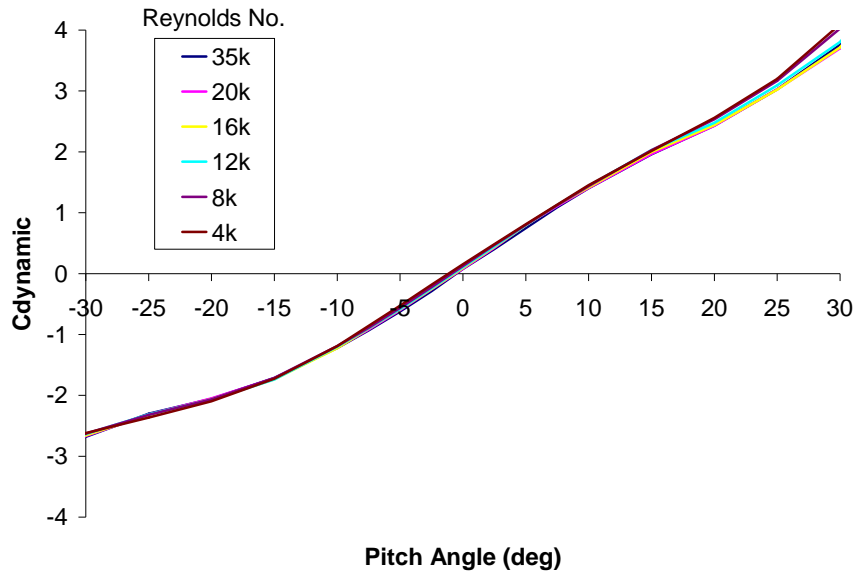


Figure 20. Pitch coefficient for ground probe. Mach 0.9, $Re=4,000$ to $35,000$, zero yaw.